Bigi, D., et al., 2022, Are fluid inclusions in gypsum reliable paleoenvironmental indicators? An assessment of the evidence from the Messinian evaporites: Geology, https://doi.org/10.1130/G49475.1

ARE FLUID INCLUSIONS IN GYPSUM RELIABLE PALEOENVIROMENTAL INDICATORS?

AN ASSESSMENT OF THE EVIDENCE FROM THE MESSINIAN EVAPORITES

SUPPLEMENTARY INFORMATION

Bigi D.[1*], Lugli S.[2], Manzi V.[1], Roveri M.[1]

[1]*University of Parma, Italy*

[2]*University of Modena and Reggio Emilia, Italy*

[*] *diego.bigi@unipr.it*

The Messinian salinity crisis

The CIESM age model

The Messinian salinity crisis (MSC; 5.97-5.33 Ma; CIESM, 2008; Roveri et al., 2014 and reference therein) can be subdivided into three main stages characterized by the accumulation of different evaporitic deposits (Fig. DR1). During stage 1 bottom grown gypsum selenite (PLG) accumulated in the shallow marginal basins of the Mediterranean. During stage 2 evaporite deposition shifted in the deeper basins and was mainly characterized by the deposition of km-thick halite deposits. During the stage 3, again sulphate evaporites (UG) were deposited in the shallow basins.

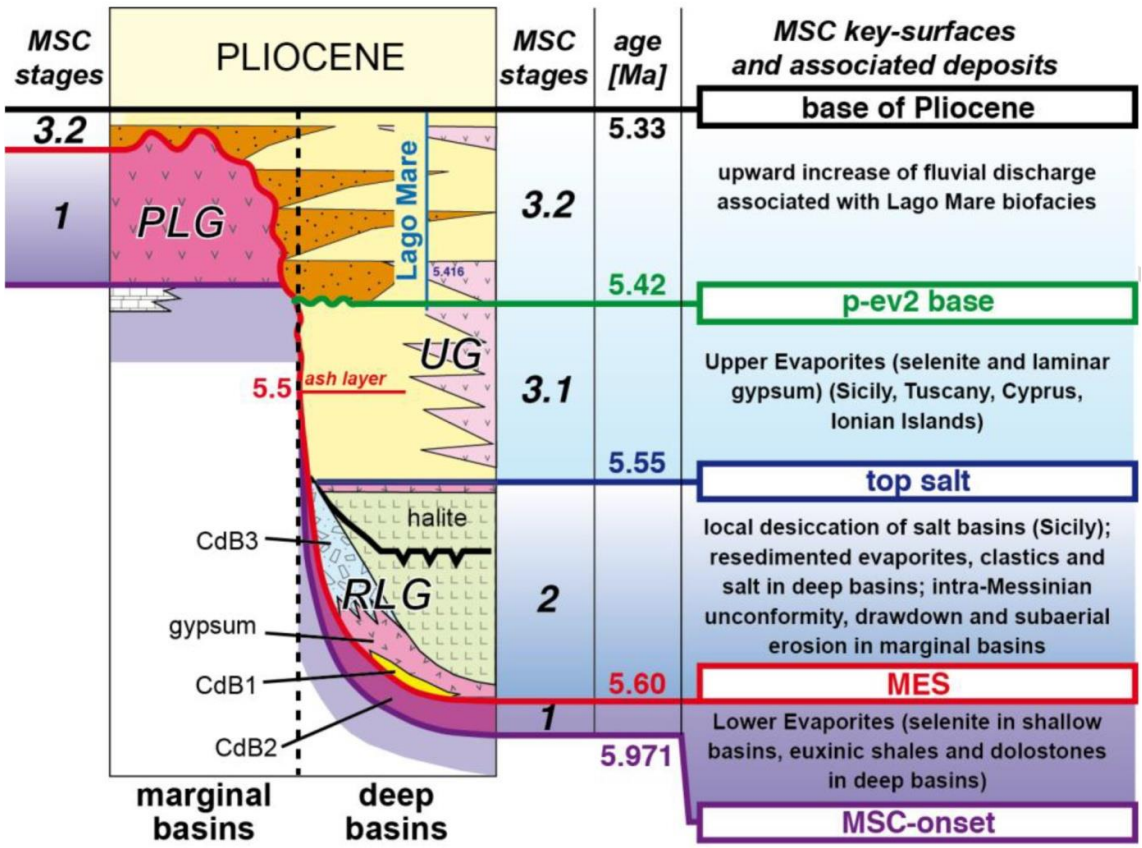

Figure DR1 – Age model of the Messinian salinity crisis (CIESM, 2008; Roveri et al., 2014b).

The Mediterranean curve of the Strontium isotope ratio during the MSC

The peculiar hydrogeological evolution of the Mediterranean shows a detachment from the global ocean, only partial during stage 1 and 2, and almost complete during stage 3 of the Messinian salinity crisis. This has been reconstructed from the $^{87}Sr/^{86}Sr$ geochemistry of evaporites (gypsum and halite), foraminifers, molluscs, ostracods and carbonates (Roveri et al., 2014b; Reghizzi et al., 2018). A main change occurred at the transition between stage 2 and 3 according to the CIESM (2008) age model and later modifications (Roveri

et al., 2014a). A main stratigraphic implication of this shift is the possibility to discriminate between the primary gypsum selenite deposits of the PLG and UG units.

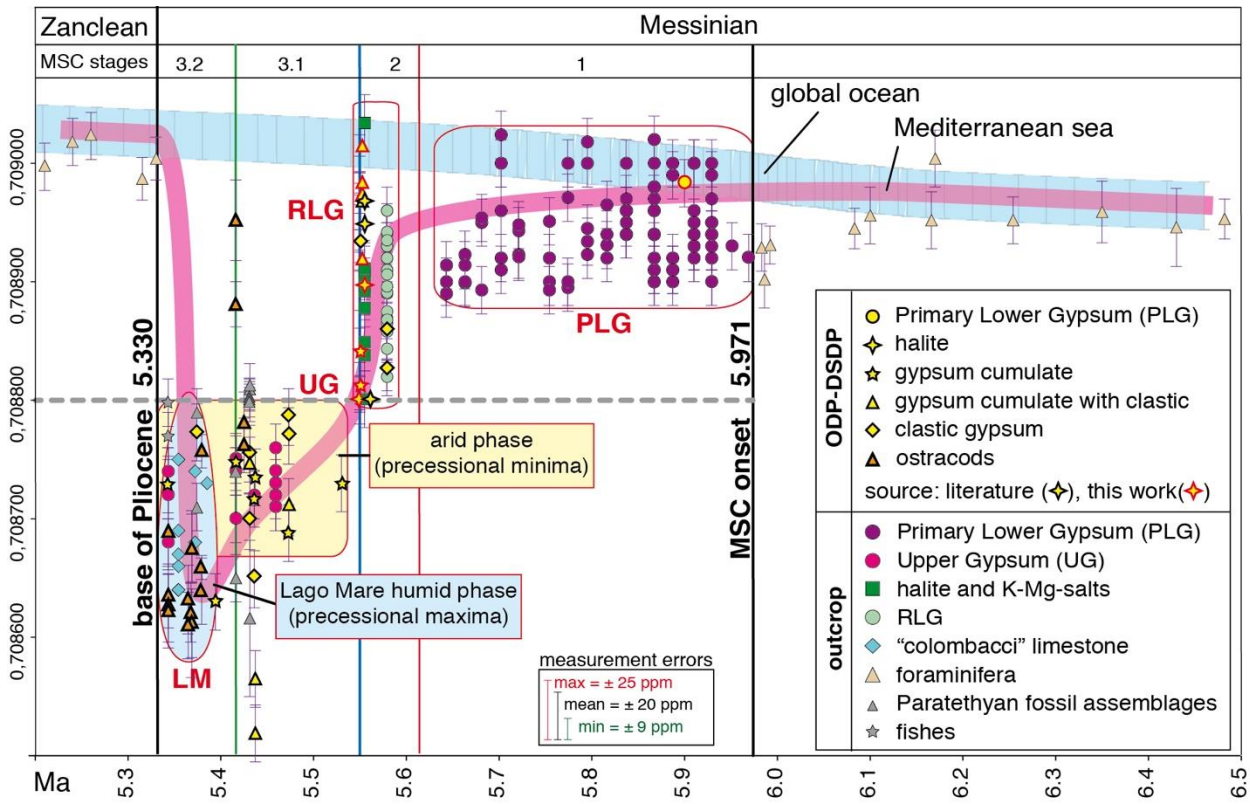

FIG. DR2 Strontium isotope curve after Roveri et al., 2014b.

Geological settings and sampling

We collected 10 samples from the PLG and 2 samples from the UG units (Tab. 1) in 9 stratigraphic sections throughout the entire Mediterranean basin (Fig. DR3).

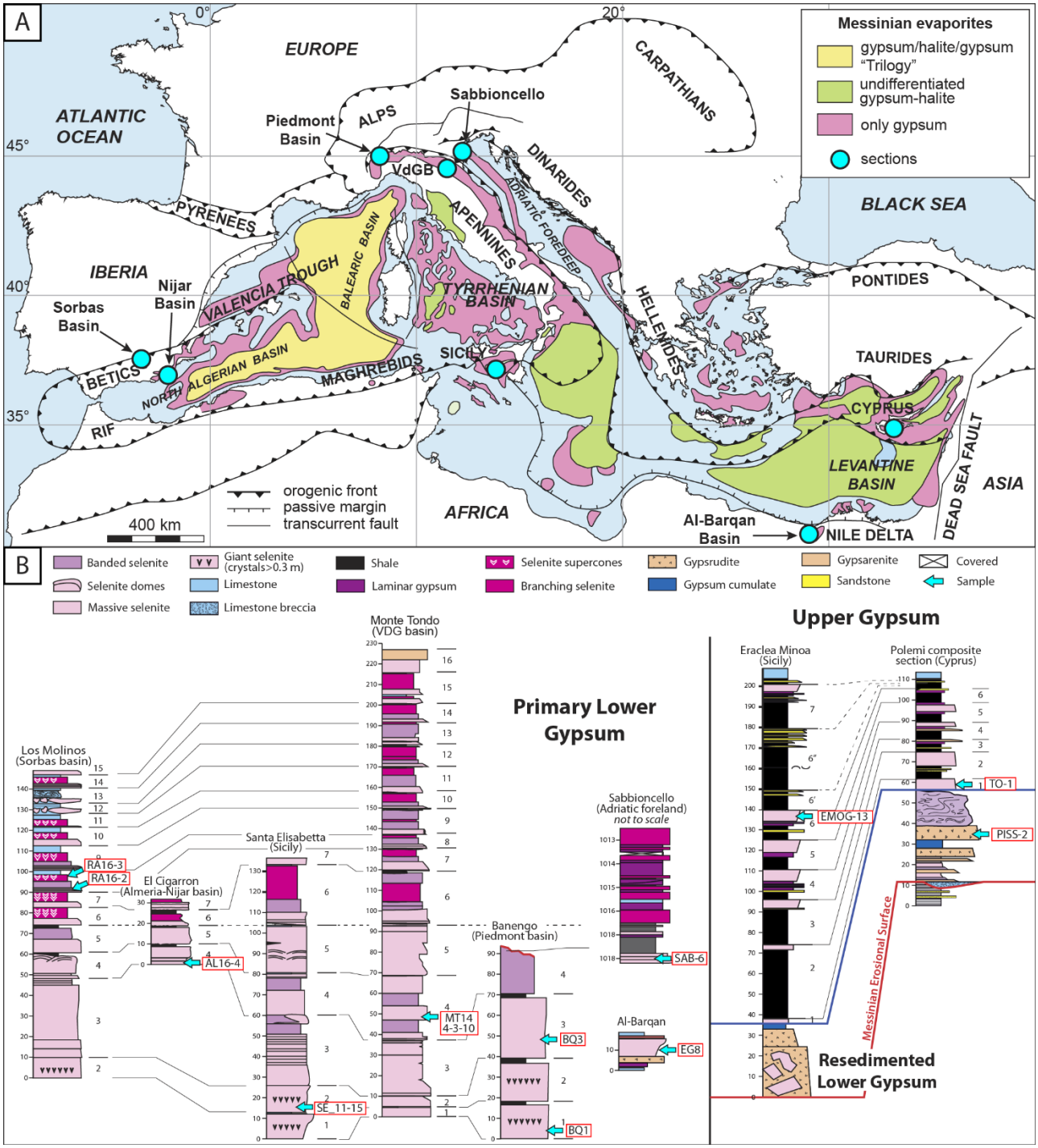

Fig. DR3 – A) Distribution of the Messinian evaporites in the Mediterranean region with the sections investigated in this work (modified from Roveri et al., 2014); Samples are from outcropping sections except for the Sabbioncello borehole. B) Stratigraphic setting and depositional facies of the samples (modified from Lugli et al., 2010; Manzi et al., 2009,2016).

The PLG samples come from Spain (Sorbas and Almeria-Nijar basins), Northern Italy (Piedmont and Vena del Gesso basins and Sabbioncello well in the Adriatic foreland), Sicily (Caltanissetta basin),

Egypt (Al-Barqan area) and Cyprus (Pissouri basin). The UG samples come from Sicily (Caltanissetta basin) and from Cyprus (Tochni basin).

Spain

The Sorbas basin contains one of the best-preserved Messinian successions. In particular, the Yesares Member (Caños Formation) is one of the most complete PLG section of the Mediterranean. We collected 2 samples of massive and branching selenite from the Rio de Aguas section exposing 3 cycles (PLG 8, 9, 10; Lugli et al., 2010). In Fig. 2 we report the more complete Los Molinos section. We have sampled the 8th cycle, the same one studied by Evans et al. (2015), which was reported by them as the 6th. In the Almeria-Nijar basin, we sampled the PLG4 massive selenite from the El Cigarron section (Fig. DR1) showing 4 cycles (from PLG 4 to PLG 7; Reghizzi, 2017).

Northern Italy

In the Tertiary Piedmont basin, the PLG unit did not preserve the original coherent stratigraphy due to the combined action of faulting and gravitative processes; In large sectors of the basin both units are unconformably overlain by the Valle Versa chaotic complex, including gypsum and carbonate olistoliths, ranging in size from meters to several hundred of meters (Dela Pierre et al., 2007). We collect PLG 1 massive selenite samples from the Banengo quarry (Fig. DR1) in the Norther sector of the basin.

The Vena del Gesso basin hosts one of the most extensive PLG successions in terms of stratigraphic record and lateral continuity. The unit is partially truncated at the top by the Messinian Erosional Surface (MES), but the Mt. Tondo section shows the complete PLG succession with all the 16 cycles and total thickness of 230 meters (Fig. DR1; Lugli et al., 2010). Here we sampled the PLG 4 massive selenite and PLG 8-9 displacive selenite.

The Sabbioncello well was drilled near the city of Ferrara. The log intercepts a thin PLG horizon at a depth between 1012 and 1020 meters. The PLG deposition in the Adriatic foreland occurred at structural highs of the more external thrust of the Apennine chain. We sampled the massive selenite.

Sicily

We collected samples from the PLG2 massive selenite at St. Elisabetta section (Agrigento, Fig. DR1; Lugli et al.,2010), and the UG6 banded selenite from Eraclea Minoa section, which represent the most complete record of the Upper Gypsum unit.

Egypt

The Egypt Miocene succession crops out in the northern part of the Western Desert (Attia et al., 2004). In the Al-Barqan and Gebel Hagif areas, the Messinian evaporites are represented by two gypsum beds (~ 11 meters thick) truncated on top by an unconformity. This gypsum unit can be correlated with the PLG unit based on $^{87}Sr/^{86}Sr$ ratio provided by this work. We have collected massive selenite samples from the Al-Barqan section (Fig. DR1; Attia et al., 2004).

Cyprus

Based on the Polemi composite section (Manzi et al., 2016), the evaporites of the Kalavasos Formation can be divided into 3 units. The lower (mainly gypsarenite and gypsrudite beds) and the intermediate ("Marmara" chaotic - laminar gypsum) units are part of the Resedimented Lower Gypsum (RLG - stage 2). The upper unit containing only bottom growth selenite facies, corresponds to the Upper Gypsum unit (UG - stage 3) and shows up to 6 gypsum-marls couplets with Lago-Mare facies associations (Manzi et al., 2016). There is no evidence of PLG preserved *in situ*, but only scattered gypsum blocks included in gypsrudite beds in the lower unit of the Kalavasos Fm. We sampled the massive selenite from PLG blocks in the Pissouri basin and the UG 1 massive selenite from the Tokhni basin.

Materials and methods

Sr Isotope analyseis

Two samples from Al-Barqan (Egypt) and Eraclea Minoa (Sicily) have been prepared for Sr geochemical analysis at the Isotope Geochemistry Laboratory at the Department of Chemical and Geological Sciences of the University of Modena and Reggio Emilia. $^{87}Sr/^{86}Sr$ ratio was gained through a multicollector inductively coupled plasma mass spectrometer (*HR-MC-ICPMS Thermo Scientific™ Neptune*) at CIGS (Centro Interdipartimentale Grandi Strumenti, University of Modena and Reggio Emilia). We followed the analytical procedure described in Reghizzi et al. (2018). Below we report the mean value of the NIST SRM 987, the 2SD uncertainty (twice standard deviation) and the number of standards for the two analytical sessions performed: Egypt session (0.710250 ± 0.000010, *n* = 11), Almeria session (0.710282 ± 0.000010, *n* = 20). The 2SE (twice standard error) on individual standard analyses varied between 0.000004 and 0.000014 (Egypt), and between 0.000005 and 0.000010 (Almeria).

Microthermometric analysis

Microthermometry was conducted using a calibrated Linkam THMS 600 heating-freezing stage mounted on a Leica transmitted light microscope with a 100x objective, at the Fluid Inclusion Laboratory, Parma University. We measured Tm_{ice} (temperature of last ice melting) from primary fluid inclusions in the lateral growth bands and in the re-entrant angle of the gypsum twins. The analytical method reports several changes compared to previous studies.

A total of 46 millimetre-sized fragments were obtained by cleaving crystals along the perfect 010 cleavage plane with a razor blade. The inclusions were subjected to mechanical stretch through multiple cooling-heating cycles with the aim of nucleating a vapor bubble. This procedure is designed to eliminate metastability, which is essential to be able to make the measurements. All previous studies report only one stress cycle, from -90 to +30 °C, at a rate of 30 °C/min. After just one cycle, however, only a very small fraction of the target inclusions nucleates a bubble and can be measured. To nucleate the bubble from a larger population of fluid inclusions we performed a stronger stress phase, increasing the cycle number (up to 9), the rate of temperature change (50 °C/m) and the temperature range (-100 to +120 °C). No evidence of gypsum dehydration has been observed except for a few cases only at the edges of the gypsum fragments. This is because of the very short permanence of the sample at peak temperature during the stress cycles. During measurement runs commonly the vapor bubble disappeared during freezing and nucleated again during heating, but only after ice melting. This is a clear indication of metastability of the system.

To yield correct Tm_{ice} values, the presence of vapor phase is needed before the last ice crystal is melted (Roedder E., 1984). Therefore, stress cycles were not sufficient to achieve the desired stability, but a variable pause at room temperature normally allowed to reach a new low-pressure equilibrium. The duration of this interval probably depends on the fluid inclusions starting pressure conditions. The time required to reach stable conditions ranged from 1 day to 3 weeks even for inclusion from the same sample.

The measurement runs were done according to previous studies (Natalicchio et al., 2014): the inclusions were frozen at -90°C at the rate of 30°C/min. Subsequently they were slowly heated following the method reported by Attia et al., 1995 until the Tm_{ice} is reached. Tm_{ice} values were converted in salinity as equivalent weight ‰ NaCl with the equation of Bodnar (1993). All the Tm_{ice} values obtained have a reproducibility of ±0.2°C and this value did not change even after 3 weeks after applying the stress. These results indicate that no water loss occurred from the FI by applying extreme stress cycles.

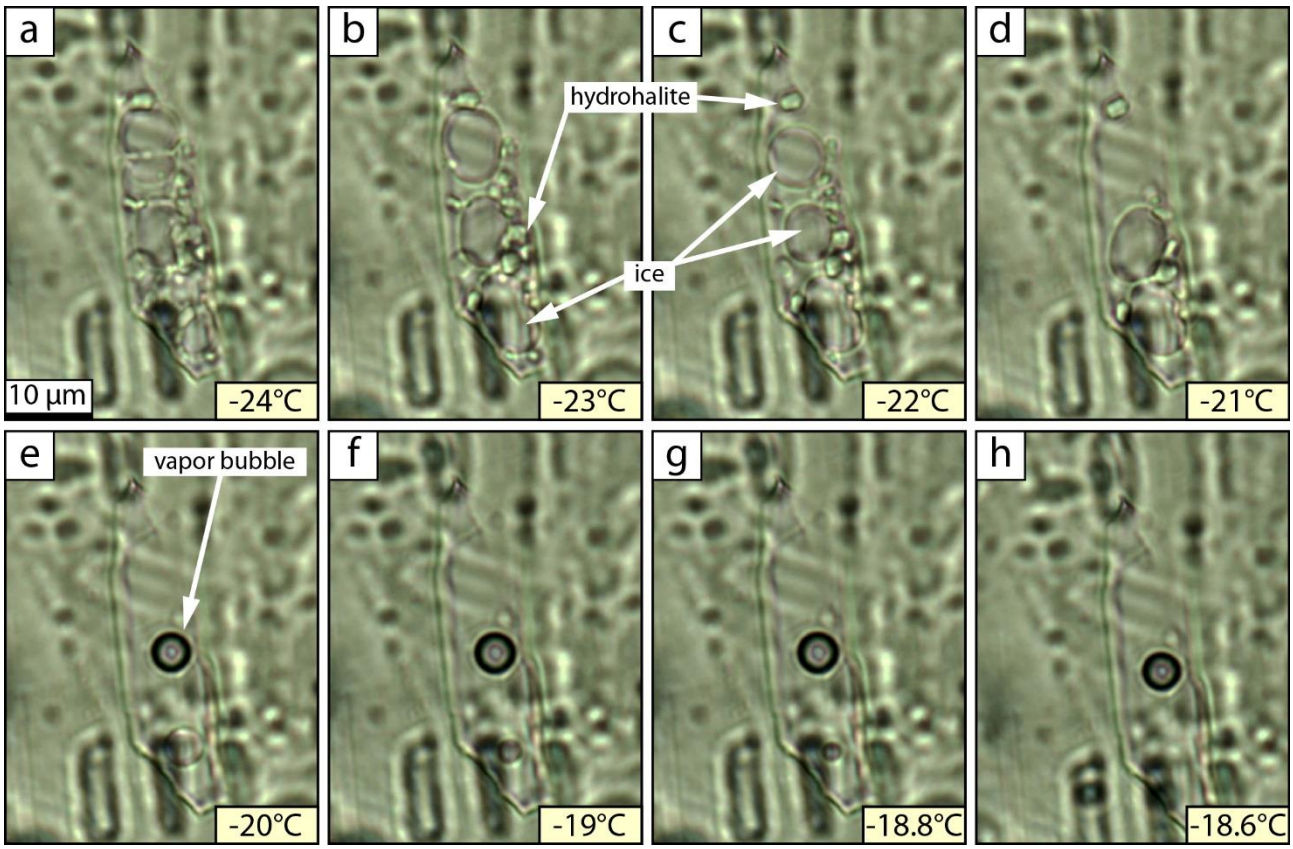

Fig. DR4 – Time lapse during slow heating (0.1 °C/min) of a fluid inclusion. a) Crystallization of hydrohalite between ice crystals. b,c,d) Progressive melting of both ice (darker) and hydrohalite (clearer, high relief) crystals. e) Complete melting of hydrohalite and nucleation of a vapor bubble. f,g,h) Progressive melting of the last ice crystal until the Tmice at -18.6.

Results

Strontium isotope analyses

The $^{87}Sr/^{86}Sr$ ratio obtained from the Al-Barqan (Egypt) and the Eraclea Minoa (Sicily) samples confirm that they belongs respectively to the PLG and UG units, according to the Mediterranean curve of Roveri et al., (2014b)(Fig. DR2). In Tab. DR1 the results of the geochemical analyses have been reported together with previous data from the literature.

Table DR1 – Sr isotope composition of the collected samples. The Sorbas basin values are from Evans et al. (2015; E15) for, the Cyprus values from Manzi et al. (2016; M16) and the VDG values from Reghizzi (2017; R17), Reghizzi et al. (2018; R18), Lugli et al. (2007; L07), and Garcia-Veigas et al. (2018; GV18). The blue-colored Sr data are from this work to discriminate the PLG from the UG units. Location information (in decimal degrees) are also reported. EG8 has the least precise coordinates: the most reliable values are from Youssef, 1988. Gypsum facies: MS, massive selenite; DS displacive selenite; BS, branching selenite.

Sample	Basin	Section	Unit	Cycle	Facies	$^{87}Sr/^{86}Sr$	Error [10^{-6}]	LAT LON	BIBLIO
RA16-2	Sorbas	Rio de Aguas	PLG	8	MS	0,708951	20	37.089777 2.115055	E15
RA16-3	Sorbas	Rio de Aguas	PLG	8	BS	0,708971	20	37.089777 2.115055	E15
AL16-4	Almeria-Nijar	El Cigarron	PLG	4	MS	0,708948	5	36.945836 -2.433613	R17
BQ1+BQ3	Piedmont	Banengo	PLG	1	MS	-	-	45.071818 8.056659	-
MT14_4-3-10	VDG	Mt. Tondo	PLG	4	MS	0.708971	7	44.251141 11.670855	R18
MT-49	VDG	Mt. Tondo	PLG	9	DS	0.708920	20	44.251141 11.670855	L07
SAB-6	Adriatic foreland	Sabbioncello	PLG	-	MS	-	-	44.829277 13.552969	-
SE_11-15	Caltanissetta	St. Elisabetta	PLG	2	MS	0.708932	-	37.089777 2.115055	GV18
EMOG-13	Caltanissetta	Eraclea Minoa	UG	6	MS	0,708760	20	37.394172 13.288710	this work
EG8	Al-Barqan	Al-Barqan	PLG	-	MS	0,708946	5	30.91 29.16 to 29.5	this work
PISS-2	Pissouri	Pissouri	PLG block in RLG	-	MS	0.708843	20	34.676597 32.667744	M16
TO-1	Psematismenos	Tochni	UG	1	MS	0.708795	20	34.768266 33.325430	M16

Microthermometric analyses

The complete record of the microthermometric measures is attached at the end of the document (Tab. DR3), here we report a summary of the measures.

Table DR2 – Summary of all microthermometric data.

Sample	Basin	Section	Cycle	Facies	N° of fragments	F.I. type	N° of F.I.	Salinity wt ‰ NaCl eq.		
								min	max	mean
RA16-2	Sorbas	Rio de Aguas	PLG8	MS	3	A/B	52	21	224	129
RA16-3	Sorbas	Rio de Aguas	PLG8	BS	4	A	29	30	229	85
AL16-4	Nijar	El-Cigarron	PLG4	MS	5	B	43	33	232	116
BQ1	Piedmont	Banengo	PLG1	MS	12	A	59	38	218	130
BQ3	Piedmont	Banengo	PLG3	MS	2	B	41	9	175	79
MT14_4-3-10	VDG	Mt. Tondo	PLG4	MS	4	B	55	40	229	149
MT-49	VDG	Mt. Tondo	PLG8/9	DS	3	A/B	39	69	235	115
SAB-6	Adriatic foreland	Sabbioncello	PLG	MS	2	B	47	37	230	126
EG-8	Al-Barqan	Al-Barqan	PLG	MS	6	B	69	34	202	145
SE_11-15	Caltanissetta	St. Elisabetta	PLG2	MS	3	A	44	45	185	92
EMOG-13	Caltanissetta	Eraclea Minoa	UG6	MS	2	B	43	108	195	151
TO-1	Psematismenos	Tokhni	UG1	MS	5	B	31	42	223	127
PISS-2	Pissouri	Pissouri	RLG(PLG)	MS	4	A/B	42	24	146	81

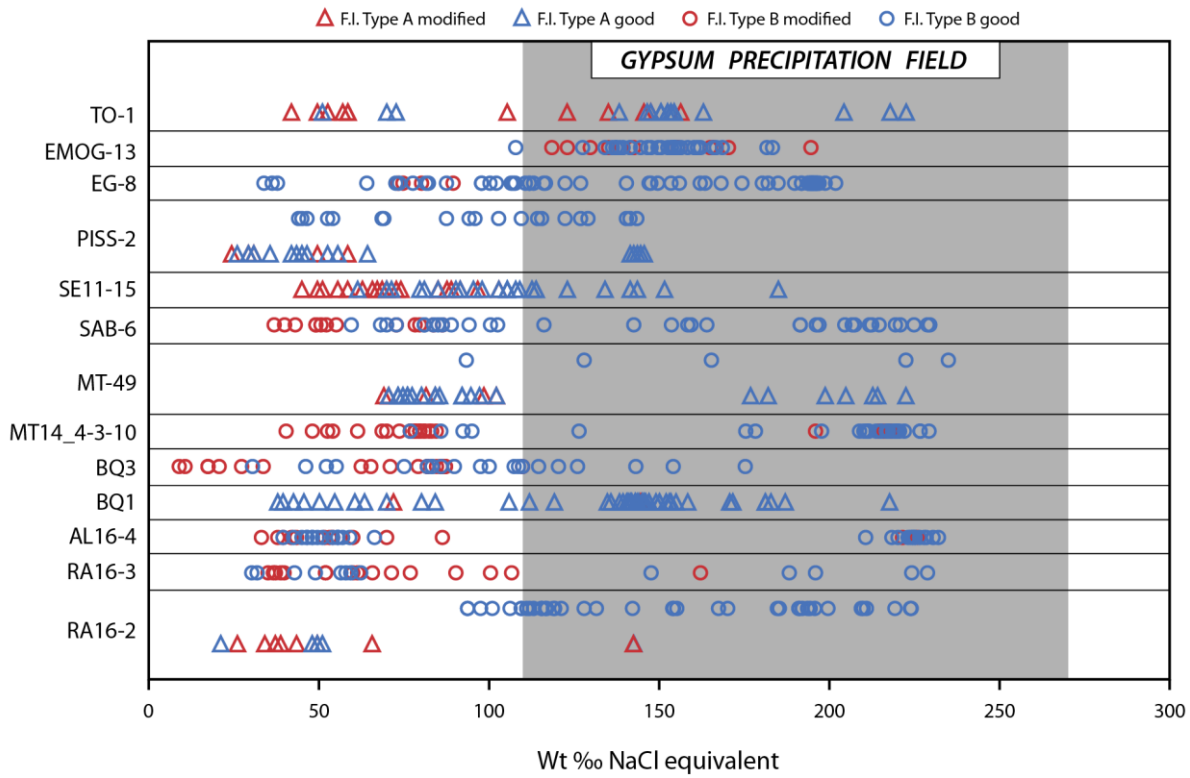

Fig. DR5. Linear distribution of salinity values for each sample. The inclusions are divided into two types: A (triangles) and type B (circles). Inclusions marked in red show evidence of post-depositional modification, whereas inclusions marked in blue are unaffected.

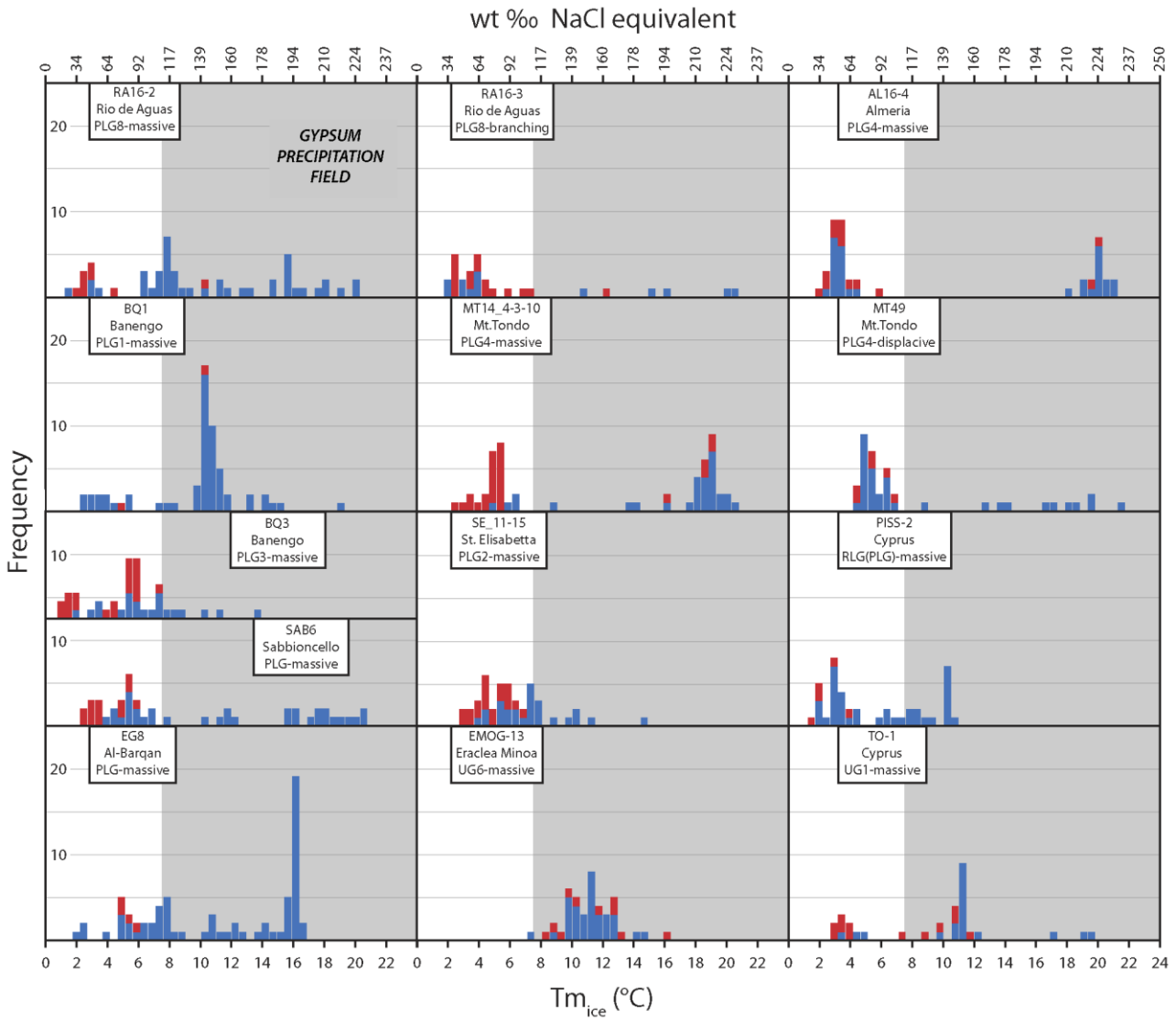

Fig.DR6 – Frequency by temperature classes of 0.5 °C for all samples. Red bars indicate inclusions with evidence of post-depositional modifications., the blue bars consist of apparently unmodified inclusions. The Upper Gypsum sample from Eraclea Minoa is the only showing a clear frequency peak.

References

Attia, O.E., Lowenstein, T.K., Wali, A.M.A., 1995; Middle Miocene gypsum, Gulf of Suez: marine or nonmarine?: Journal of Sedimentary. Research, v. 65A, p. 614–626.

Attia, O.E., El Khoriby E., Aref M. A., 2004, Sedimentology and fluid inclusions criteria of the Upper Miocene (Messinian?) gypsum deposits in the Mediterranean coast of Egypt: Sedimentology of Egypt, v. 12, p. 23–39.

Bodnar, R., 1993, Revised equation and table for determining the freezing point de-pression of H2O–Nacl solutions: Geochimica et Cosmochimica Acta, v. 57, p. 683–684.

Dela Pierre, F., Festa, A., Irace, A., 2007, Interaction of tectonic, sedimentary and diapiric processes in the origin of chaotic sediments: an example from the Messinian of Torino Hill (Tertiary Piedmont Basin, northwestern Italy): Geological Society of America Bulletin, v. 119, p. 1107–1119, doi:10.1130/B26072.1.

García-Veigas, J., Cendon, D.L., Gibert, L., Lowenstein, T.K., Artiaga, D., 2018, Geo-chemical indicators in Western Mediterranean Messinian evaporites: implications for the salinity crisis: Marine Geology, v. 403, p. 197–214, doi:10.1016/j.margeo.2018.06.005.

Lugli, S., Bassetti, M.A., Manzi, V., Barbieri, M., Longinelli, A., Roveri, M., 2007, The Messinian 'Vena del Gesso' evaporites revisited: characterization of isotopic composition and organic matter: Geological Society (Londra) Special Publication, v.285, p. 179–190, doi:10.1144/SP285.11.

Lugli, S., Manzi, V., Roveri, M., Schreiber, B.C., 2010, The Primary Lower Gypsum in the Mediterranean: a new facies interpretation for the first stage of the Messinian salinity crisis: Palaeogeography, Palaeoclimatology, Palaeoecology, v. 297, p. 83–99, doi:10.1016/j.palaeo.2010.07.017.

Manzi, V., Lugli, S., Roveri, M., Schreiber, B.C., 2009, A new facies model for the Upper Gypsum (Sicily, Italy): chronological and paleoenvironmental constraints for the Messinian salinity crisis in the Mediterranean: Sedimentology, v. 56, p. 1937–1960, doi:10.1111/j.1365-3091.2009.01063.x.

Manzi, V., Lugli, S., Roveri, M., Dela Pierre, F., Gennari, R., Lozar, F., et al. (2016), The Messinian salinity crisis in Cyprus: A further step towards a new stratigraphic framework for eastern Mediterranean: Basin Research, v. 28, p. 207–236, doi:10.1111/bre.12107.

Natalicchio, M., Dela Pierre, F., Lugli, S., Lowenstein, T.K., Feiner, S.J., Ferrando, S., Manzi, V., Roveri, M., Clari, P., 2014, Did Late Miocene (Messinian) gypsum precipitate from evaporated marine brines? Insights from the Piedmont Basin (Italy): Geology, v. 42, p. 179–182, doi: 10.1130/G34986.1.

Reghizzi, 2017, Ciclicità sub-milankoviana nelle Evaporiti Messiniane: analisi sedimentologiche, petrografiche, geochimiche e geochimico-isotopiche [Ph.D thesis]: Parma, University of Parma, 178 p.

198 Reghizzi, M., Lugli, S., Manzi, V., Rossi, F.P., Roveri, M., 2018, Orbitally forced hydro-logical balance during
199 the Messinian Salinity Crisis: insights from strontium iso-topes (87Sr/86Sr) in the Vena del Gesso Basin
200 (Northern Apennines, Italy): Paleoceanography and Paleoclimatology, v.33, p. 716–731,
201 doi:10.1029/2018PA003395.

202 Roedder, E. 1984, Fluid Inclusions: Reviews in Mineralogy, Mineralogical Society of America, v. 12, p. 291-
203 304.

204 Roveri, M., Flecker, R., Krijgsman, W., Lofi, J., Lugli, S., Manzi, V., Sierro, F.J., Bertini, A., Camerlenghi, A., De
205 Lange, G., Govers, R., Hilgen, F.J., Hübscher, C., Meijer, P.T., Stoica, M., 2014a, The Messinian Salinity Crisis:
206 past and future of a great challenge for marine sciences: Marine Geology, v. 352, p. 25–58,
207 doi:10.1016/j.margeo.2014.02.002.

208 Roveri, M., Lugli, S., Manzi, V., Gennari, R., Schreiber, B.C., 2014b, High-resolution strontium isotope
209 stratigraphy of the Messinian deep Mediterranean basins: implications for marginal to central basins
210 correlation: Marine Geology, v. 349, p. 113–125, doi:10.1016/j.margeo.2014.01.002.

211 Youssef E. A. A., 1988, Sedimentological studies of Neogene evaporites in the northern Western Desert ,
212 Egypt: Sedimentary Geology, v. 59, p. 261-273.

Microthermometric analyses complete results

Table DR3 Microthermometric analyses complete results

RA16-2 (Sorbas - Rio de Aguas, PLG8, massive selenite).					
Fragment	**F.I. type**	**Tm_{ice} (°C)**	**wt ‰ NaCl**	**Size (µm²)**	**Leakage**
SB1b	B	-14,9	185	182	
SB1b	B	-16,2	196	168	
SB1b	B	-9,0	128	40	
SB1b	B	-11,4	154	65	
SB1b	B	-7,9	115	65	
SB1b	B	-7,4	110	377	
SB1b	B	-7,9	115	225	
SB1b	B	-8,2	119	352	
SB1b	B	-8,4	121	360	
SB1b	B	-7,6	112	350	
SB1b	B	-7,7	113	240	
SB1b	B	-6,7	101	741	
SB1b	B	-7,4	110	152	
SB1b	B	-20,0	224	175	
SB1b	B	-16,7	200	300	
SB1b	B	-8,0	117	188	
SB1b	B	-18,0	210	221	
SB1b	B	-15,6	191	225	
SB1c	B	-10,3	142	102	
SB1c	B	-20,0	224	95	
SB1c	B	-16,0	194	273	
SB1c	B	-19,4	219	72	
SB1c	B	-15,7	192	63	
SB1c	B	-15,6	191	100	
SB1c	B	-13,1	170	120	
SB1c	B	-11,5	154	96	
SB1c	B	-18,0	209	68	
SB1c	B	-18,2	211	92	
SB1c	B	-15,9	194	150	
SB1c	B	-14,8	185	120	
SB1c	B	-12,8	167	100	
SB1c	B	-11,6	155	168	
SB1c	B	-9,3	132	144	
SB1c	B	-8,2	119	174	
SB1c	B	-7,1	106	108	
SB1c	B	-8,0	117	68	
SB1c	B	-6,4	98	126	
SB1c	B	-7,5	111	216	
SB1c	B	-6,1	94	273	
SB1c	B	-6,1	94	273	
SB1k	B	-10,3	143	147	✓
SB1k	B	-1,2	21	560	
SB1k	B	-3,1	51	595	
SB1k	B	-3,0	50	848	
SB1k	B	-2,2	37	2848	✓
SB1k	B	-2,6	43	3638	✓
SB1k	B	-4,1	66	612	✓
SB1k	B	-3,0	50	563	✓
SB1k	B	-2,3	39	2310	✓
SB1k	B	-2,9	48	720	
SB1k	B	-1,5	26	450	✓
SB1k	B	-2,0	34	9377	✓
RA16-3 (Sorbas - Rio de Aguas, PLG8, selenite branching selenite “supercones”).					
Fragment	**F.I. type**	**Tm_{ice} (°C)**	**wt ‰ NaCl**	**Size (µm²)**	**Leakage**
R1a	A	-3,2	52	1697	✓
R1a	A	-2,1	35	796	✓
R1a	A	-3,2	52	168	✓
R1a	A	-3,6	58	44	
R1a	A	-3,5	56	44	
R1a	A	-3,7	59	44	
R1a	A	-16,2	196	64	
R1b	A	-3,0	49	168	

R1b	A	-2,6	43	30	
R1b	A	-3,9	62	60	
R1b	A	-1,8	30	105	
R1b	A	-1,9	32	266	
R1b	A	-2,4	40	168	✓
R1b	A	-2,2	37	240	✓
R5	A	-15,2	188	102	
R6	A	-2,2	37	300	✓
R6	A	-12,3	162	36	✓
R6	A	-4,5	71	84	✓
R6	A	-7,1	107	145	✓
R6	A	-2,3	39	144	✓
R6	A	-5,9	90	338	✓
R6	A	-20,1	224	64	
R6	A	-10,8	148	88	
R6	A	-6,7	100	364	✓
R6	A	-3,8	61	693	✓
R6	A	-3,7	60	3850	✓
R6	A	-4,1	66	2650	✓
R6	A	-4,9	77	560	✓
R6	A	-20,8	229	12	
AL16-4 (Nijar – El-Cigarron, PLG4, massive selenite).					
Fragment	**F.I. type**	**Tm_{ice} (°C)**	**wt ‰ NaCl**	**Size (µm²)**	**Leakage**
AL-4-1a	B	-21,3	232	451	
AL-4-1a	B	-19,5	220	456	
AL-4-1a	B	-19,7	222	348	✓
AL-4-1a	B	-2,5	42	319	✓
AL-4-1a	B	-2,8	47	1220	
AL-4-1a	B	-2,7	45	1122	
AL-4-1a	B	-2,8	47	507	
AL-4-1a	B	-3,5	57	880	
AL-4-1a	B	-3,1	51	11899	
AL-4-1a	B	-2,9	48	2511	
AL-4-1a	B	-3,4	56	920	
AL-4-1a	B	-2,9	48	680	
AL-4-1a	B	-2,6	43	855	✓
AL-4-1a	B	-3,4	56	1081	
AL-4-1a	B	-3,7	60	1518	✓
AL-4-1a	B	-3,0	50	2568	
AL-4-1a	B	-3,3	54	988	
AL-4-1a	B	-3,4	56	444	
AL-4-1b	B	-5,6	86	756	✓
AL-4-1b	B	-4,4	70	3264	✓
AL-4-1b	B	-3,3	54	9342	✓
AL-4-2q	B	-2,3	38	270	✓
AL-4-2i	B	-2,3	39	650	✓
AL-4-2i	B	-19,9	223	88	
AL-4-2i	B	-21,0	231	217	
AL-4-2i	B	-2,5	43	1377	
AL-4-2i	B	-2,3	39	576	
AL-4-2i	B	-3,2	53	1316	✓
AL-4-2i	B	-4,1	66	72	
AL-4-2i	B	-3,6	59	70	
AL-4-2i	B	-2,0	33	157,5	✓
AL-4-2i	B	-3,1	52	525	✓
AL-4-2i	B	-20,6	228	48	
AL-4-2i	B	-20,7	229	88	
AL-4-2i	B	-20,3	226	288	✓
AL-4-2i	B	-20,2	225	102	
AL-4-2i	B	-20,1	225	54	
AL-4-2i	B	-20,2	225	110	
AL-4-2i	B	-20,0	224	110	
AL-4-2i	B	-20,4	227	99	
AL-4-2i	B	-20,1	225	66	
AL-4-2i	B	-18,1	211	135	
AL-4-aa	B	-19,2	218	135	
BQ1+BQ3 (Piedmont – Banengo, PLG1,3, massive selenite).					
Fragment	**F.I. type**	**Tm_{ice} (°C)**	**wt ‰ NaCl**	**Size (µm²)**	**Leakage**
BQ1-1d	A	-13,3	172	182	

BQ1-1d	A	-11,4	154	66	
BQ1-1d	A	-10,6	146	44	
BQ1-1g	A	-10,1	141	144	
BQ1-1g	A	-7,6	112	70	
BQ1-1g	A	-10,2	142	240	
BQ1-1g	A	-10,1	141	325	
BQ1-1h	A	-11,5	155	187	
BQ1-1i	A	-8,2	119	504	
BQ1-1l	A	-9,7	136	99	
BQ1-1l	A	-9,6	135	80	
BQ1-2b	A	-13,2	171	56	
BQ1-2f	A	-10,6	146	108	
BQ1-2f	A	-10,4	144	308	
BQ1-2h	A	-11,9	158	90	
BQ1-2m	A	-10,2	142	54	
BQ1-2m	A	-10,0	139	99	
BQ1-2m	A	-9,9	138	130	
BQ1-2m	A	-10,1	140	72	
BQ1-2m	A	-10,5	145	176	✓
BQ1-2m	A	-10,2	142	40	
BQ1-2m	A	-10,6	146	70	
BQ1-2m	A	-4,4	70	162	
BQ1-3a	A	-3,9	63	96	
BQ1-3a	A	-5,1	80	169	
BQ1-3a	A	-3,7	61	98	
BQ1-3a	A	-2,3	39	575	
BQ1-3b	A	-5,4	84	252	
BQ1-3b	A	-10,7	147	56	
BQ1-3b	A	-10,2	142	144	
BQ1-3b	A	-2,7	46	1140	
BQ1-3b	A	-7,1	106	480	
BQ1-3b	A	-10,1	141	304	
BQ1-3b	A	-4,5	72	298	✓
BQ1-3b	A	-10,3	143	234	
BQ1-3b	A	-11,0	150	63	
BQ1-3b	A	-10,3	143	240	
BQ1-3b	A	-2,3	38	456	
BQ1-3b	A	-10,4	144	195	
BQ1-3b	A	-10,3	143	308	
BQ1-3b	A	-3,0	50	1089	
BQ1-3b	A	-10,7	147	140	
BQ1-3b	A	-3,3	55	347	
BQ1-3b	A	-2,5	43	165	
BQ1-3b	A	-10,6	146	180	
BQ1-3b	A	-10,3	143	195	
BQ1-3b	A	-11,2	152	400	
BQ1-3b	A	-10,4	144	156	
BQ1-3b	A	-10,5	145	110	
BQ1-3b	A	-10,5	145	99	
BQ1-4	A	-14,6	183	61	
BQ1-4	A	-10,9	149	54	
BQ1-4	A	-19,1	218	35	
BQ1-4	A	-11,0	150	81	
BQ1-4	A	-11,3	153	40	
BQ1-4	A	-14,4	181	66	
BQ1-4	A	-15,1	187	30	
BQ1-4	A	-14,4	181	56	
BQ1-4	A	-10,5	145	64	
BQ3-1b	B	-8,3	120	210	
BQ3-1b	B	-10,4	143	120	
BQ3-1b	B	-8,8	126	80	
BQ3-1b	B	-5,5	86	1254	
BQ3-1b	B	-5,6	87	312	✓
BQ3-1b	B	-7,3	109	240	
BQ3-1b	B	-7,4	110	153	
BQ3-1b	B	-5,4	85	338	✓
BQ3-1b	B	-5,5	86	2112	✓
BQ3-1b	B	-5,2	82	430	✓
BQ3-1b	B	-5,5	86	130	✓
BQ3-1b	B	-5,6	87	522	✓

BQ3-1b	B	-1,6	27	1452	✓
BQ3-1b	B	-5,2	82	1225	✓
BQ3-1b	B	-3,4	55	286	
BQ3-1b	B	-5,0	79	336	✓
BQ3-1b	B	-3,9	62	1715	✓
BQ3-1b	B	-5,3	83	1044	
BQ3-1b	B	-0,5	9	1782	✓
BQ3-1b	B	-7,8	115	160	
BQ3-1b	B	-5,5	86	744	✓
BQ3-1b	B	-6,6	100	360	
BQ3-1b	B	-5,2	82	952	
BQ3-1b	B	-0,6	11	1020	✓
BQ3-1b	B	-4,1	65	940	✓
BQ3-1b	B	-5,3	83	100	
BQ3-1b	B	-4,5	71	864	✓
BQ3-1b	B	-4,7	75	84	
BQ3-1b	B	-7,4	110	1218	✓
BQ3-1b	B	-3,2	52	864	
BQ3-1b	B	-1,2	21	1280	✓
BQ3-1b	B	-1,0	17	3575	✓
BQ3-1b	B	-2,0	34	5640	✓
BQ3-1b	B	-1,0	17	10384	✓
BQ3-2a	B	-6,4	98	624	
BQ3-2a	B	-5,8	90	156	
BQ3-2a	B	-7,2	107	21	
BQ3-2a	B	-1,8	30	2068	
BQ3-2a	B	-2,8	46	680	
BQ3-2a	B	-11,4	154	70	
BQ3-2a	B	-13,7	175	96	
MT14_4-3-10 (Vena Del Gesso – Mt. Tondo, PLG4, massive selenite					
Fragment	**F.I. type**	**Tm_{ice} (°C)**	**wt ‰ NaCl**	**Size (µm²)**	**Leakage**
VG1a	B	-18,2	210,9	216	
VG1a	B	-19,1	217,3	209	
VG1a	B	-19,7	222,0	105	
VG1a	B	-6,2	95,0	315	
VG1a	B	-6,0	92,4	1269	
VG1a	B	-20,8	229,4	75	
VG1a	B	-20,4	226,7	65	
VG1a	B	-19,1	217,3	189	✓
VG1a	B	-18,3	211,6	84	
VG1a	B	-20,4	226,7	66	
VG1a	B	-5,3	83,2	1300	✓
VG1a	B	-5,4	84,5	1558	✓
VG1a	B	-13,7	175,4	60	
VG1a	B	-5,5	85,9	496	
VG1a	B	-4,6	73,6	11421	✓
VG1b	B	-18,1	210,2	182	
VG1b	B	-19,2	217,9	120	✓
VG1b	B	-16,2	196,0	168	✓
VG1b	B	-19,3	218,6	102	
VG1b	B	-19,6	220,7	119	
VG1b	B	-19,5	220,0	65	
VG1b	B	-19,5	220,0	78	
VG1b	B	-19,4	219,3	90	
VG1b	B	-18,3	211,6	60	
VG1b	B	-18,6	213,8	66	
VG1b	B	-18,8	215,2	50	
VG1a	B	-5,2	81,0	6985	✓
VG1a	B	-5,1	79,6	731	✓
VG1a	B	-2,9	48,0	928	✓
VG1a	B	-4,9	76,9	1480	✓
VG1a	B	-5,0	78,3	4848	✓
VG1a	B	-5,3	82,3	3612	✓
VG1a	B	-5,1	79,6	630	✓
VG1a	B	-5,1	79,6	858	✓
VG1a	B	-4,9	76,9	902	✓
VG1a	B	-4,3	68,6	9000	✓
VG1a	B	-5,2	81,0	3555	✓
VG1a	B	-3,8	61,4	4505	✓
VG1a	B	-3,3	54,1	4275	✓

VG1a	B	-4,4	70,0	1539	✓
VG1a	B	-4,9	76,9	1634	
VG1a	B	-5,0	78,3	1014	✓
VG1a	B	-5,0	78,3	1235	✓
VG1a	B	-8,8	126,4	364	
VG1a	B	-16,4	197,8	78	
VG1a	B	-18,9	216,0	110	✓
VG1a	B	-18,7	214,6	132	✓
VG1a	B	-14,1	178,3	91	
VG1a	B	-19,0	216,7	77	
VG1a	B	-19,1	217,4	88	
VG1a	B	-2,4	40,4	468	✓
VG1a	B	-17,9	208,9	66	
VG1a	B	-18,8	215,3	104	
VG1a	B	-3,2	52,6	924	✓
T2d	B	-19,1	217,4	171	
MT-49 (Vena Del Gesso – Mt. Tondo, PLG 9, displacive selenite).					
Fragment	**F.I. type**	**Tm_{ice} (°C)**	**wt ‰ NaCl**	**Size (µm²)**	**Leakage**
M3b	A	-5,1	80,2	221	
M3b	A	-4,8	76,1	420	
M3b	A	-4,6	73,3	391	
M3b	A	-4,6	73,3	242	
M3b	A	-4,6	73,3	400	
M3b	A	-4,7	74,7	208	
M3b	A	-4,8	76,1	272	
M3b	A	-4,4	70,5	192	
M3b	A	-5,4	84,2	180	
M3b	A	-4,3	69,1	2397	✓
M3b	A	-5,4	84,2	84	
M3b	A	-5,5	85,5	198	
M3b	A	-13,9	176,9	91	
M3b	A	-18,4	212,8	66	
M3b	A	-18,6	214,2	153	
M3b	A	-16,6	198,9	224	
M3b	A	-5,4	84,2	576	✓
M3b	A	-6,8	102,2	480	
M3b	A	-4,8	76,1	825	
M3b	A	-14,5	182,0	136	
M3b	A	-4,4	70,5	506	✓
M3b	A	-5,1	80,2	180	
M3b	A	-4,8	76,1	418	
M3b	A	-4,9	77,4	480	
M3b	A	-6,8	102,2	1015	✓
M3b	A	-6,0	92,1	135	
M3b	A	-5,4	84,2	88	
M3b	B	-12,6	165,4	112	
M3b	B	-9,0	128,0	198	
M3c	B	-6,1	93,4	513	
M3c	B	-21,7	235,0	130	
M3y	A	-6,4	97,2	260	
M3y	A	-17,4	204,9	90	
M3y	A	-19,8	222,5	36	
M3y	A	-5,2	81,6	138	✓
M3y	A	-6,2	94,7	54	
M3y	A	-6,0	92,1	84	
M3y	A	-6,5	98,5	420	✓
M3y	B	-19,8	222,5	56	
SAB-6 (Adriatic foreland – Sabbioncello log, PLG, massive selenite).					
Fragment	**F.I. type**	**Tm_{ice} (°C)**	**wt ‰ NaCl**	**Size (µm²)**	**Leakage**
F6a	B	-20,9	230	152	
F6a	B	-5,1	80	696	✓
F6a	B	-12,5	164	138	
F6a	B	-7,9	116	52	
F6a	B	-6,7	100	429	
F6a	B	-5,5	85	170	
F6a	B	-6,2	94	105	
F6a	B	-5,4	84	561	✓
F6a	B	-15,6	192	92	
F6a	B	-18,4	213	105	

F6a	B	-5,2	81	204	
F6a	B	-4,4	70	357	
F6a	B	-5,6	86	1015	✓
F6a	B	-20,8	229	171	
F6a	B	-5,2	81	210	
F6a	B	-5,4	84	136	
F6a	B	-5,8	89	315	
F6a	B	-5,6	86	360	
F6a	B	-4,6	73	825	✓
F6a	B	-17,6	207	140	
F6a	B	-16,3	197	90	
F6a	B	-17,3	205	91	
F6a	B	-20,2	225	105	
F6a	B	-16,2	196	135	
F6a	B	-12,0	159	220	
F6a	B	-11,9	158	216	
F6a	B	-10,3	143	60	
F6a	B	-11,4	154	180	
F6a	B	-5,0	78	1173	✓
F6a	B	-15,6	192	55	
F6a	B	-19,4	220	72	
F6a	B	-17,7	207	48	
F6a	B	-18,7	215	60	
F6a	B	-18,3	212	95	
F6a	B	-19,6	221	310	
F6a	B	-4,6	73	507	
F6a	B	-3,0	49	403	✓
F6a	B	-2,2	37	408	✓
F6a	B	-3,0	49	416	✓
F6a	B	-3,2	52	494	✓
F6a	B	-3,1	51	384	✓
F6a	B	-2,4	40	270	✓
F6a	B	-2,6	43	768	✓
F6b	B	-4,3	68	300	
F6b	B	-6,8	103	165	
F6b	B	-3,7	60	805	
F6b	B	-3,4	55	1040	✓
SE11-15 (Sicily – St. Elisabetta, PLG2, massive selenite).					
Fragment	**F.I. type**	**Tm_{ice} (°C)**	**wt ‰ NaCl**	**Size (µm²)**	**Leakage**
Se11-15a	A	-5,2	81,0	368	
Se11-15a	A	-10,2	141,5	132	
Se11-15a	A	-5,5	85,0	224	✓
Se11-15a	A	-3,1	51,1	352	✓
Se11-15a	A	-4,1	65,7	1672	✓
Se11-15a	A	-4,2	67,1	918	✓
Se11-15b	A	-6,8	103,0	187	
Se11-15b	A	-8,5	123,1	50	
Se11-15b	A	-7,2	107,8	176	
Se11-15b	A	-7,0	105,4	40	
Se11-15b	A	-5,9	90,3	143	
Se11-15b	A	-7,7	113,8	42	
Se11-15b	A	-6,3	95,4	374	
Se11-15b	A	-6,4	96,7	494	✓
Se11-15b	A	-6,0	91,6	130	✓
Se11-15b	A	-5,7	87,6	4218	✓
Se11-15b	A	-5,1	79,6	2170	
Se11-15b	A	-4,6	72,8	864	✓
Se11-15b	A	-3,0	49,6	4107	✓
Se11-15b	A	-4,4	70,0	1241	
Se11-15b	A	-5,8	89,0	1680	✓
Se11-15b	A	-2,7	45,0	2117,5	✓
Se11-15c	A	-3,9	62,8	170	✓
Se11-15c	A	-3,4	55,5	80	✓
Se11-15c	A	-5,5	85,0	169	✓
Se11-15c	A	-4,4	70,0	240	✓
Se11-15c	A	-3,8	61,4	120	
Se11-15c	A	-6,5	98,0	1980	
Se11-15c	A	-3,6	58,5	1287	✓
Se11-15c	A	-7,0	105,4	32	
Se11-15c	A	-6,8	103,0	300	✓

Se11-15c	A	-4,7	74,1	1457	✓
Se11-15c	A	-4,5	71,4	1763	
Se11-15c	A	-6,0	91,6	90	
Se11-15c	A	-7,6	112,6	324	
Se11-15c	A	-14,8	185,0	28	
Se11-15c	A	-10,4	143,6	156	
Se11-15c	A	-7,0	105,4	54	
Se11-15c	A	-4,3	68,6	290	✓
Se11-15c	A	-5,5	85,0	283,5	
Se11-15c	A	-7,7	113,8	480	
Se11-15c	A	-9,5	134,1	399	
Se11-15c	A	-11,2	151,6	12	
Se11-15c	A	-7,3	109,1	126	
PISS-2 (Cyprus – Pissouri, RLG(PLG), massive selenite).					
Fragment	**F.I. type**	**Tm_{ice} (°C)**	**wt ‰ NaCl**	**Size (µm²)**	**Leakage**
P4a	B	-9,1	129,1	247	
P4a	B	-7,4	109,5	216	
P4a	B	-4,3	69,1	616	
P4a	B	-2,6	44,0	624	
P4a	B	-7,9	115,5	90	
P4a	B	-7,8	114,3	70	
P4a	B	-8,5	122,4	540	
P4a	B	-8,9	126,9	385	
P4a	B	-6,3	95,9	304	
P4a	B	-6,8	102,8	288	
P4a	B	-10,2	141,4	280	
P4a	B	-5,7	87,5	1044	
P4a	B	-10,4	143,5	144	
P4a	B	-10,1	140,4	432	
P4e	B	-2,8	46,5	55	
P4e	B	-4,3	68,6	187	
P4e	B	-6,2	94,1	120	
P4e	B	-3,3	54,1	98	
P4e	B	-3,2	52,6	96	
P4e	B	-2,7	45,0	272	
P2g	B	-10,6	145,6	216	
P2g	B	-1,7	29,3	1599	✓
P2g	B	-10,4	143,6	315	
P2g	B	-10,5	144,6	165	
P2g	B	-3,0	49,6	1560	✓
P2g	B	-3,6	58,5	529	✓
P2g	B	-1,5	26,0	12000	
P4d	A	-1,4	24,4	468	✓
P4d	A	-10,2	141,5	60,5	
P4d	A	-10,3	142,6	108	
P2e	A	-1,7	29,3	1813	
P2e	A	-1,8	30,9	1824	✓
P2e	A	-3,4	55,5	5040	
P2e	A	-3,2	52,6	558	
P2e	A	-2,7	45,0	290	
P2e	A	-4,0	64,3	665	
P2e	A	-1,8	30,9	3445	
P2e	A	-2,1	35,7	1176	
P2e	A	-2,5	41,9	260	
P2e	A	-2,6	43,5	357	
P2e	A	-2,8	46,5	924	
EG8 (Egypt – Al-Barqan, PLG, massive selenite).					
Fragment	**F.I. type**	**Tm_{ice} (°C)**	**wt ‰ NaCl**	**Size (µm²)**	**Leakage**
EG8w	B	-4,6	73,6	98	
EG8w	B	-16,1	195,5	65	
EG8w	B	-16,3	197,1	40	
EG8w	B	-4,9	77,7	44	
EG8w	B	-12,9	168,2	54	
EG8w	B	-16,2	196,3	144	
EG8w	B	-15,9	194,0	72	
EG8w	B	-8,5	122,4	85	
EG8w	B	-7,5	110,7	375	
EG8w	B	-7,6	111,9	180	
EG8w	B	-6,8	102,2	216	

EG8z	B	-4,7	74,7	512	✓
EG8z	B	-4,6	73,3	418	✓
EG8z	B	-5,1	80,2	2368	✓
EG8y	B	-2,2	37,8	80	
EG8y	B	-16,1	195,0	105	
EG8y	B	-14,3	180,4	330	
EG8y	B	-16,1	195,0	85	
EG8y	B	-15,7	191,8	243	
EG8y	B	-15,7	191,8	264	
EG8y	B	-14,5	182,0	168	
EG8y	B	-2,1	36,3	286	
EG8j	B	-5,8	89,5	368	✓
EG8j	B	-8,0	116,6	136	
EG8j	B	-7,2	107,1	612	
EG8j	B	-7,7	113,1	396	
EG8j	B	-7,6	111,9	720	
EG8j	B	-13,6	174,3	120	
EG8j	B	-17,0	201,9	124	
EG8j	B	-5,2	81,5	40	
EG8j	B	-10,7	147,0	153	
EG8j	B	-8,9	126,9	176	
EG8j	B	-12,4	163,5	288	
EG8j	B	-16,6	198,9	100	
EG8j	B	-11,6	155,9	90	
EG8k	B	-6,4	97,8	294	
EG8k	B	-7,2	107,7	168	
EG8k	B	-11,4	153,5	160	
EG8k	B	-7,1	106,5	190	
EG8k	B	-11,0	149,6	125	
EG8k	B	-10,1	140,4	100	
EG8k	B	-5,7	87,5	880	
EG8k	B	-7,9	116,1	90	
EG8k	B	-14,8	185,0	100	
EG8k	B	-4,6	72,6	266	
EG8k	B	-6,6	100,3	720	
EG8k	B	-6,4	97,8	180	
EG8u	B	-10,8	147,6	315	
EG8u	B	-15,4	189,8	230	
EG8u	B	-15,9	193,8	124	
EG8u	B	-2,0	33,9	288	
EG8u	B	-4,0	64,1	574	
EG8u	B	-5,3	82,2	300	
EG8u	B	-12,3	162,1	288	
EG8u	B	-15,9	193,8	39	
EG8u	B	-16,0	194,6	288	
EG8u	B	-16,1	195,4	147	
EG8u	B	-16,1	195,4	90	
EG8u	B	-16,2	196,2	100	
EG8u	B	-16,3	196,9	130	
EG8u	B	-16,0	194,6	198	
EG8u	B	-16,1	195,4	120	
EG8u	B	-16,0	194,6	165	
EG8u	B	-16,1	195,4	132	
EG8u	B	-16,2	196,2	55	
EG8u	B	-16,0	194,6	160	
EG8u	B	-16,0	194,6	210	
EG8u	B	-16,2	196,2	112	
EG8u	B	-16,2	196,2	154	

EMOG-13 (Sicily – Eraclea Minoa, UG6, massive selenite).

Fragment	F.I. type	Tm_{ice} (°C)	wt ‰ NaCl	Size (µm²)	Leakage
EMOG-13-1a	B	-8,5	123	184	✓
EMOG-13-1a	B	-7,2	108	45	
EMOG-13-1a	B	-8,1	118	232	✓
EMOG-13-1a	B	-12,2	161	35	
EMOG-13-1a	B	-11,9	158	119	
EMOG-13-1a	B	-10,5	145	195	
EMOG-13-1a	B	-12,7	166	60	
EMOG-13-1a	B	-11,7	157	48	
EMOG-13-1a	B	-11,5	155	40	
EMOG-13-1a	B	-11,6	156	49	

EMOG-13-1a	B	-14,6	183	64	
EMOG-13-1a	B	-11,0	150	55	
EMOG-13-1a	B	-11,5	155	70	
EMOG-13-1a	B	-10,8	148	72	
EMOG-13-1a	B	-12,3	162	48	
EMOG-13-1a	B	-11,4	154	40	
EMOG-13-1a	B	-12,1	160	48	
EMOG-13-1a	B	-9,9	138	65	
EMOG-13-1a	B	-10,7	147	60	
EMOG-13-1a	B	-11,5	155	72	
EMOG-13-1a	B	-9,8	137	45	
EMOG-13-1a	B	-10,0	139	45	
EMOG-13-1a	B	-9,7	136	60	
EMOG-13-1a	B	-9,5	134	50	
EMOG-13-1a	B	-10,2	142	60	
EMOG-13-1b	B	-12,6	165	84	✓
EMOG-13-1b	B	-11,4	154	110	
EMOG-13-1b	B	-9,1	130	66	✓
EMOG-13-1b	B	-11,1	151	40	
EMOG-13-1b	B	-16,0	195	32	✓
EMOG-13-1b	B	-14,4	182	48	
EMOG-13-1b	B	-11,5	155	56	
EMOG-13-1b	B	-11,6	156	288	✓
EMOG-13-1b	B	-12,8	167	90	
EMOG-13-1b	B	-13,0	169	378	
EMOG-13-1b	B	-12,7	166	264	✓
EMOG-13-1b	B	-13,2	170	405	✓
EMOG-13-1b	B	-10,3	143	287,5	✓
EMOG-13-1b	B	-11,3	153	80	
EMOG-13-1b	B	-10,2	142	130	
EMOG-13-1b	B	-9,8	137	60	
EMOG-13-1b	B	-9,6	135	266	✓
EMOG-13-1b	B	-8,9	128	132	

TO-1 (Cyprus – Tokhni, UG1, massive selenite).					
Fragment	**F.I. type**	**Tm_{ice} (°C)**	**wt ‰ NaCl**	**Size (µm²)**	**Leakage**
TO-1d	A	-11,7	157	117	✓
TO-1d	A	-11,4	154	90	
TO-1d	A	-4,6	73	82	
TO-1e	A	-11,5	155	88	
TO-1e	A	-11,4	154	84	
TO-1e	A	-11,3	153	35	
TO-1e	A	-9,9	138	170	
TO-1e	A	-11,5	155	112	
TO-1e	A	-11,3	153	192	
TO-1f	A	-10,7	147	68	
TO-1f	A	-8,5	123	132	✓
TO-1a	A	-12,4	163	88	
TO-1a	A	-10,8	148	152	
TO-1a	A	-7,0	105	273	✓
TO-1a	A	-17,3	205	45	
TO-1a	A	-11,1	151	126	
TO-1a	A	-11,1	151	35	
TO-1g	A	-9,6	135	112	✓
TO-1g	A	-19,2	218	144	
TO-1g	A	-10,6	146	330	✓
TO-1g	A	-10,8	148	119	✓
TO-1g	A	-11,1	151	570	
TO-1g	A	-19,9	223	154	
TO-1a	A	-3,6	58	104	✓
TO-1f	A	-3,0	50	3800	✓
TO-1f	A	-4,4	70	710,5	
TO-1f	A	-3,6	58	2968	✓
TO-1f	A	-3,2	53	2254	✓
TO-1f	A	-3,5	57	1593	✓
TO-1f	A	-3,1	51	432	
TO-1f	A	-2,5	42	275,5	✓